

# Influence of the magnetic material on tunneling magnetoresistance and spin-transfer torque in tunnel junctions: *Ab initio* studies

Christian Franz, Michael Czerner, and Christian Heiliger<sup>1,\*</sup>

<sup>1</sup>*I. Physikalisches Institut, Justus Liebig University, Giessen, Germany*

(Dated: May 25, 2022)

The dependence of tunneling magnetoresistance and spin-transfer torque in FeCo/MgO/FeCo tunnel junctions on the Co concentration and the bias voltage are investigated *ab initio*. We find that the tunneling magnetoresistance decreases with the Co concentration in contradiction with previous calculations but in agreement with recent experiments. This dependence is explained from bulk properties of the alloys. By using a realistic description of the disorder in the alloys we can show that even small amounts of disorder lead to a drastic drop in the tunneling magnetoresistance. This provides a quantitative explanation of the difference between calculated and measured values.

The spin-transfer torque shows a linear voltage dependence for the in-plane component and a quadratic for the out-of-plane component for all concentrations at small bias voltages. In particular, the linear slope of the in-plane torque is independent of the concentration. For high bias voltages the in-plane torque shows a strong nonlinear deviation from the linear slope for high Co concentrations. This is explained from the same effects which govern the tunneling magnetoresistance.

PACS numbers: 85.75.-d, 73.63.-b, 75.70.Cn, 71.15.Mb

## I. INTRODUCTION

Tunneling magnetoresistance (TMR)<sup>1,2</sup> occurs in junctions consisting of two ferromagnetic layers separated by an insulator. TMR is the change of resistance of the tunnel junction due to changing the relative orientation between the two magnetizations of the ferromagnetic leads. A number of applications such as hard-disk-drive read heads, sensors, and magnetic random access memory (MRAM) exploit the effect of TMR. Typical TMR ratios exceed several hundred percent in crystalline MgO based tunnel junctions<sup>3–5</sup> as predicted theoretically<sup>6,7</sup>.

In order to use a magnetic tunnel junction as a storage element in MRAM an efficient way of writing information is required, i.e. of switching the magnetization in one of the layers (free layer). Driving a current through a tunnel device can switch the magnetic orientation of a ferromagnetic layer. Thereby, one exploits the effect of spin-transfer torque (STT) which was predicted by Slonczewski<sup>8,9</sup> and Berger<sup>10</sup>. The current gets spin-polarized in one ferromagnetic layer, tunnels through the barrier, and enters the second ferromagnetic layer. If the magnetization of the second ferromagnetic layer is not perfectly aligned with the polarization of the current, even due to thermal fluctuations, the transport electrons start to precess around the exchange field of the second ferromagnetic layer. This in turn leads to a STT acting on the magnetization of this ferromagnetic layer. If the current is large enough the magnetization can be reversed. For smaller currents the magnetization oscillates, which can be used to create a microwave oscillator<sup>11</sup>.

There is a large interest in understanding the behavior of STT in tunnel junctions because this effect is a promising way to advance the development of MRAM applications<sup>12</sup>. The critical current where the magnetization switches is the crucial quantity for applications. However, to lower the critical current one needs to un-

derstand the basic physics, in particular the bias dependence of the STT and the dependence on material parameters. Experimental results show different bias dependencies<sup>13,14</sup>. In particular, Kubota *et al.*<sup>14</sup> observe a nonlinear bias dependence of the in-plane STT supported by simple model calculations<sup>15,16</sup>. In contrast, Sankey *et al.*<sup>13</sup> find a linear dependence of the in-plane STT supported by *ab initio* calculations<sup>17</sup>. Recent experimental investigations by Wang *et al.*<sup>18</sup> suggest that these differences in the previous experimental results arise from the analysis of the resonance functions, in particular the dependence on the magnetic offset angles. A detailed analysis<sup>18</sup> leads to interpretations supporting the *ab initio* calculations for both experiments. The experiments<sup>13,18</sup> are done with FeCo alloys for the ferromagnetic layers whereas previous *ab initio* calculations were performed using pure Fe leads. Therefore, the properties of the ferromagnetic leads in experiments and *ab initio* theory are different. This makes the agreement<sup>17</sup> appear a bit surprising. Here we show that for small voltages the linear dependence of the in-plane STT is independent of the composition of the FeCo alloy. However, for large voltages the in-plane STT shows a strong deviation from this linear dependence for large Co concentrations.

It has been demonstrated that imperfect interface structures between the ferromagnetic layer and the barrier, in particular FeO at the interface, have a strong influence on transport properties in TMR devices<sup>19</sup>. Recent model calculations show the influence of the size of the exchange splitting and the band filling in the ferromagnetic layers on the bias dependence of the STT<sup>20,21</sup>. These investigations show that the bias dependence can be drastically changed using different band parameters, which are bulk properties. One task of this article is to clarify the relative importance of bulk properties of the ferromagnetic layers and interface effects for the case of perfect interfaces. In this respect, we find that all domi-

nating effects can be understood from bulk properties.

Prior calculations investigating the TMR for different lead compositions indicate that high Co concentrations should be beneficial<sup>22</sup>. These calculations are performed at zero bias and neglect disorder in the alloy. Recent experiments however find a decrease of the TMR for large Co concentrations<sup>23,24</sup>. We show that even small amounts of disorder cause a substantial decrease of the TMR at zero bias. This provides a quantitative explanation for the difference between calculated and measured TMR values. At a large bias voltage we find that the TMR decreases with the Co concentration, in agreement with experiments. This is explained from bulk properties of the FeCo alloys.

The article is organized in the following way. First, we give a short overview over the investigated structures and the applied methods, in particular the description of the alloys, in Sec. II. In order to understand the influence of different effects we then investigate the dependence of the TMR and its bias dependence on the ferromagnetic material. The results are presented in Sec. III A. The observed high TMR ratios in FeCo/MgO/FeCo tunnel junctions are related to the STT in the same structures. The origin of the STT in tunnel junctions is explained in Sec. III B.

## II. METHOD

We investigate the different junctions shown in Fig. 1. Each junction consists of 20 monolayers (on average) FeCo on each side, separated by 6 monolayers MgO. The junction is contacted to artificial copper leads, which are in Fe-bcc structure. In order to simulate experimental thickness fluctuations, which reduce the effect of quantum well states, we average over configurations containing 50% 20 monolayers and 25% each 19 and 21 monolayers FeCo. The potentials are calculated self-consistently using a screened Korringa-Kohn-Rostoker (KKR) multiple scattering Green's function approach and a local-density approximation for the exchange-correlation potential. For the lattice structure we assume "ideal" positions: The metals have bcc structure with the equilibrium lattice constant of iron  $a_{\text{Fe}} = 0.287$  nm. The MgO is strained to  $\sqrt{2} a_{\text{Fe}} = 0.405$  nm in-plane while maintaining its equilibrium lattice constant  $a_{\text{MgO}} = 0.424$  nm out-of-plane. The Fe [100] direction is aligned with the MgO [110] direction<sup>6</sup>. The distance between iron and oxygen is 0.235 nm. Note that this structure differs from the one used in our previous studies, which was based on an experimental structure with FeO at the interface<sup>25</sup>.

The alloys are described using the coherent potential approximation (CPA)<sup>26</sup>, assuming completely disordered substitutional alloys. The CPA introduces a complex effective medium which restores the symmetry of the underlying lattice and accurately describes the scattering of Bloch waves by disorder. This leads to a finite lifetime of the Bloch states and thus to a broadening of

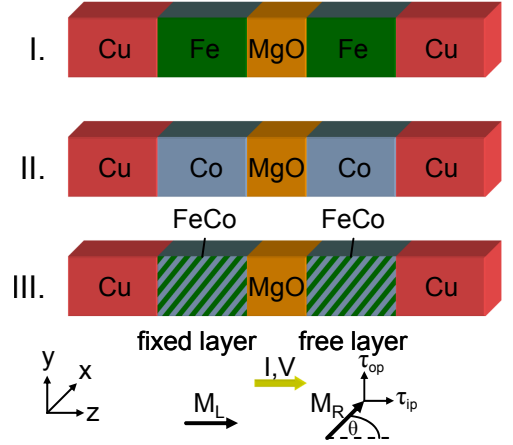


Figure 1. (Color online) Structures of the investigated tunnel junctions. In structure III the ferromagnetic layers are disordered  $\text{Fe}_{1-x}\text{Co}_x$  alloys. The left  $\vec{M}_L$  and right  $\vec{M}_R$  magnetizations of the tunnel junctions lie in the  $xz$  plane at a relative angle  $\theta$  (here  $\theta = 90^\circ$ ). We investigate the spin-transfer torque acting on the free layer  $\vec{M}_R$ , while  $\vec{M}_L$  is considered fixed. It can be divided into the in-plane torque  $\tau_{ip}$ , which lies perpendicular to  $\vec{M}_R$  in the plane defined by  $\vec{M}_L$  and  $\vec{M}_R$ , and the out-of-plane torque  $\tau_{op}$ , which points perpendicular to that plane. For a positive voltage, the electrons flow from the free layer to the fixed layer. For junction III we consider either  $\text{Fe}_{0.5}\text{Co}_{0.5}$  as an example or the full concentration dependence.

the energy bands. This can be observed in the Bloch spectral density<sup>27</sup> ( $\vec{k}$ -resolved density), see Fig. 2. The calculation of transport and non-equilibrium densities for systems containing CPA-alloys requires determination of non-equilibrium vertex corrections (NVC)<sup>28–30</sup>. The NVC describe the influence of the disorder scattering on transport properties and can be understood as accounting for the diffusive part of the current. The CPA and the NVC have recently been implemented in our KKR-method<sup>28</sup>.

The TMR is defined by the ratio

$$\frac{R_{\text{ap}} - R_{\text{p}}}{R_{\text{p}}} = \frac{I_{\text{p}} - I_{\text{ap}}}{I_{\text{ap}}} = \frac{G_{\text{p}} - G_{\text{ap}}}{G_{\text{ap}}}, \quad (1)$$

where  $R$  ( $I$ ,  $G = I/V = 1/R$ ) is the resistance (current, conductance) in the tunnel junction for fixed bias voltage  $V$  and parallel (P) or antiparallel (AP) alignment of the magnetizations in the ferromagnetic layers. The currents are calculated *ab initio* using the non-equilibrium Green's function (NEGF) formalism. Applied to the transport problem, the NEGF method yields a Landauer formula, which relates the quantum mechanical transmission coefficients  $T$  to the current. Applying a finite bias voltage results in a difference in the chemical potentials  $\mu_L/\mu_R$  in the left and right lead  $V = (\mu_R - \mu_L)/e$  and at zero

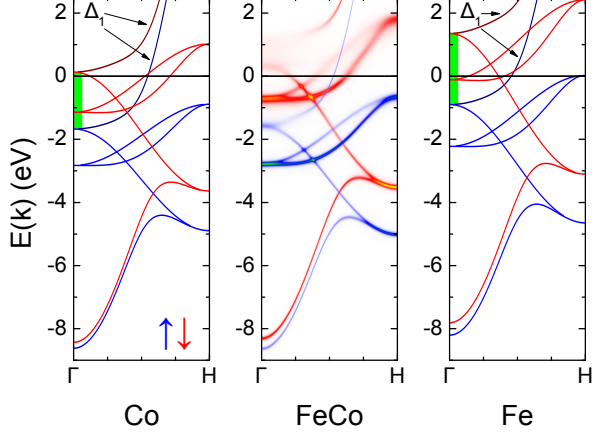


Figure 2. (Color online) Band structure of Fe and Co and Bloch spectral function of  $\text{Fe}_{0.5}\text{Co}_{0.5}$  along the  $\Delta$ -line, i.e.  $\Gamma$ -H. For Fe and Co the  $\Delta_1$ -half-metallic energy range is marked (range between the majority ( $\uparrow$ ) and minority ( $\downarrow$ )  $\Delta_1$  band).

temperature we get for the current  $I_\sigma$  in spin channel  $\sigma$

$$I_\sigma = \frac{e}{h} \int_{\mu_L}^{\mu_R} dE \sum_{\vec{k}_\parallel} T_\sigma(\vec{k}_\parallel; E), \quad (2)$$

where  $T_\sigma(\vec{k}_\parallel; E)$  is calculated from NEGFs<sup>28,31,32</sup> and  $\vec{k}_\parallel$  is summed over the 2D-Brillouin zone perpendicular to the transport direction. The voltage drop is assumed to be linear within the barrier. For the limit of zero bias the currents in Eq. (1) are replaced by the corresponding conductances, which are calculated in linear response:  $G_\sigma = \frac{e^2}{h} \sum_{\vec{k}_\parallel} T_\sigma(\vec{k}_\parallel; E_F)$ , where  $E_F$  is the Fermi-energy. Since our non-relativistic calculations do not include spin-flip scattering, we get two independent spin channels for collinear magnetizations. Thus, we have  $I_p = I_{\uparrow\uparrow} + I_{\downarrow\downarrow}$  for P and  $I_{ap} = I_{\uparrow\downarrow} + I_{\downarrow\uparrow}$  for AP alignment, where the double spin indices indicate the majority( $\uparrow$ )/minority( $\downarrow$ ) spin in the left and right lead. For alloys we get separate contributions to the transmission and current accounting for the coherent and diffusive (i.e. from the NVC) part<sup>28</sup>.

The STT consists of two contributions, the in-plane and out-of-plane torque, which are sketched in Fig. 1. The in-plane component is zero without an applied voltage whereas the out-of-plane component can be nonzero due to interlayer exchange coupling<sup>33,34</sup>. To calculate the torque  $\vec{\tau}_i$  on atomic layer  $i$ , we use the change in the magnetic moment in each layer  $\delta\vec{m}_i$  due to the current. The torque acting on atomic layer  $i$  is<sup>35</sup>

$$\vec{\tau}_i = \frac{d\vec{M}_i}{dt} = \frac{1}{\hbar} \Delta_i \hat{M}_i \times \delta\vec{m}_i, \quad (3)$$

where  $\vec{M}_i$  is the magnetic moment,  $\hat{M}_i = \frac{\vec{M}_i}{M_i}$ , and  $\Delta_i$  is the exchange energy on atomic layer  $i$ . To obtain the

total STT exerted on the free layer  $\vec{\tau}_i$  is summed over the corresponding atomic layers. We use a NEGF technique to calculate the non-equilibrium magnetic moment  $\delta\vec{m}_i$ . For more details of our method see Refs. 28, 31, and 35.

In the NEGF calculations we use a  $\vec{k}_\parallel$ -mesh of  $N_k \geq 200^2$  points. For the TMR in the pure limits we add the requirement that  $N_E N_k \geq 8 \cdot 10^5$ , where  $N_E$  is the number of energy points in the integration (Eq. (2)) to ensure convergence.

### III. RESULTS

#### A. Tunneling Magnetoresistance

It has been shown that, in order to understand the high TMR in FeCo/MgO/FeCo tunnel junctions, a quantum mechanical treatment is indispensable. It is a consequence of the symmetry-dependent transmission probability through the MgO barrier close to the Brillouin zone center and the exchange splitting<sup>5,6</sup>. The states that dominate the transport properties are of  $\Delta_1$  symmetry, i.e. states which have the full rotational symmetry of the interface ( $C_{4v}$ ). In FeCo the exchange splitting leads to an energy gap between the bottom of the majority and minority  $\Delta_1$  band which includes the Fermi-energy. This means that the  $\Delta_1$  states, which decay the most slowly in MgO, are present only for the majority spin in FeCo at the Fermi-level. This  $\Delta_1$ -half-metallic nature of FeCo leads to the high TMR ratio.

To be exact, the designation of states in terms of the  $\Delta$  representations is only valid at  $\bar{\Gamma}$ , yet we will refer to the entire bands with their character at the  $\bar{\Gamma}$  point, to simplify notation.

We will show that the major features of the TMR (and also the STT) in the considered junctions with ideal interfaces can be explained from bulk properties. The importance of the  $\Delta_1$  states is a result of the MgO complex band structure, which determines that these states have the smallest decay rate in the MgO band gap<sup>6,36</sup>. We focus on the properties of the ferromagnetic layers. Figure 2 shows the band structure of Co and Fe and the Bloch spectral function of a  $\text{Fe}_{0.5}\text{Co}_{0.5}$ -alloy along the  $\Delta$ -line, which coincides with the transport direction at the  $\bar{\Gamma}$  point in the 2D-Brillouin zone. Regarding the pure materials, we see that the change in band filling caused by one additional electron from  $^{26}\text{Fe}$  to  $^{27}\text{Co}$  leads to a shift of the Fermi-energy, in particular with respect to the  $\Delta_1$ -half-metallic region. We find that this has important consequences for the voltage dependence of TMR and STT. The exchange splitting in Co is smaller than in Fe. As explained in Sec. II, the broadening in the FeCo Bloch spectral function is a result of the disorder. This obscures the onset of the  $\Delta_1$  band and half-metallic region.

We start by investigating the concentration dependence of the TMR, calculated using Eq. (1). This is shown in Fig. 3. At zero bias the TMR drops drastically from both pure limits to finite concentrations but then remains nearly constant throughout the concentration range. At the large voltage the TMR is smaller and decreases with the Co concentration. The full voltage dependence is discussed later. In order to understand the striking dependence at zero bias we analyze the dependence of the tunneling conductance in the P and AP configuration shown in Fig. 4. The drop in the TMR is caused by an increase of the conductance in the AP configuration, while the P conductance remains roughly constant. From Fig. 4 we find that the AP conductance is completely diffusive. This indicates that the disorder

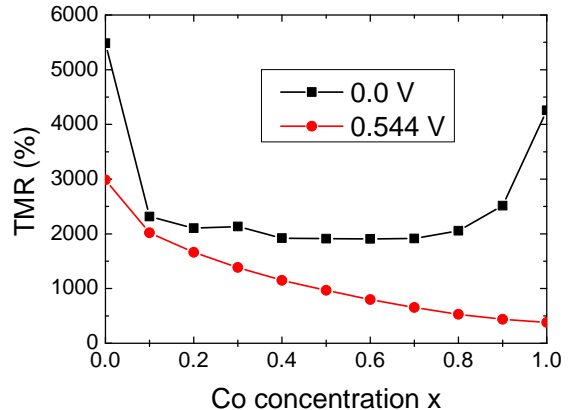


Figure 3. (Color online) Concentration dependence of the TMR for zero and a large bias voltage in  $\text{Fe}_{1-x}\text{Co}_x/\text{MgO}/\text{Fe}_{1-x}\text{Co}_x$  junctions.

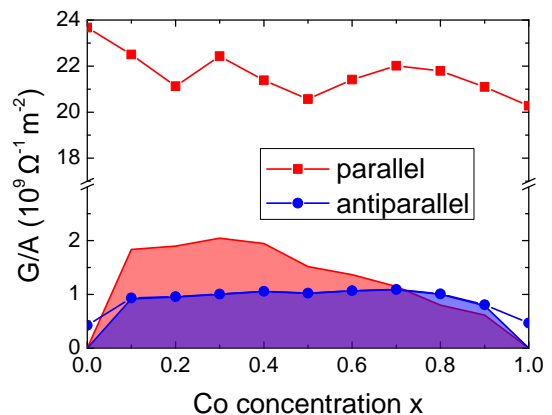


Figure 4. (Color online) Concentration dependence of the conductance in  $\text{Fe}_{1-x}\text{Co}_x/\text{MgO}/\text{Fe}_{1-x}\text{Co}_x$  junctions at zero bias voltage for P and AP alignment. The shaded area indicates the diffusive part of the conductance.

der scattering reduces the effects responsible for the high TMR.

To explicate this, we show the  $\vec{k}_{\parallel}$ -resolved transmission at zero bias in Fig. 5. This allows us to explain the origin of the large TMR in more detail. Note that for finite concentrations the effective  $\vec{k}_{\parallel}$ -resolved transmission can be understood as the ratio of incident and transmitted electrons at  $\vec{k}_{\parallel}$  within the current, where the incident and transmitted particles need not be the same. For all junctions, the P majority channel  $T_{\uparrow\uparrow}$  shows a single pronounced peak around  $\bar{\Gamma}$ . This peak consists of majority  $\Delta_1$  states, which are strongly facilitated by the MgO complex band structure in this  $\vec{k}_{\parallel}$ -region<sup>36</sup>. It adds up to a large  $G_{\uparrow\uparrow}$  conductance which dominates  $G_p$ . It is important to note that this peak cannot be explained from the  $\vec{k}_{\parallel}$ -resolved density of states (bulk

or interface) but requires knowledge of the character of the states. For Fe and Co the P minority channel  $T_{\downarrow\downarrow}$  shows a complicated structure. The gross shape can be explained from the MgO complex band structure. Most importantly, it causes the empty spot around  $\bar{\Gamma}$ , where the available minority states are suppressed. The details of  $T_{\downarrow\downarrow}$  depend on several effects, including the shape of the Fermi-surface, quantum well states, and interface resonance states. For AP alignment the majority (minority) states of the left lead tunnel to the minority (majority) states in the right lead. Since the states contributing to  $T_{\uparrow\uparrow}$  and  $T_{\downarrow\downarrow}$  are located in different  $\vec{k}_{\parallel}$ -regions they do not overlap. This leads to the strong suppression of the transmission  $T_{ap}$  in the AP alignment. Because of that, we have  $G_p \gg G_{ap}$  and thus a high TMR. Note that this requires the full  $\vec{k}_{\parallel}$ -resolved information and cannot be obtained from integrated properties. In particular, this does not require  $G_{\uparrow\uparrow} \gg G_{\downarrow\downarrow}$ , i.e. a large polarization of the P conductance.

For  $\text{Fe}_{0.5}\text{Co}_{0.5}$  we find that  $T_{\downarrow\downarrow}$  as well as  $T_{ap}$  are strongly smeared out. This is an effect of the disorder which leads to a scattering of the Bloch waves and thus redistributes the electrons across the Fermi-surface. The Fermi-surface exhibits the same broadening that is visible in the Bloch spectral density. In  $T_{\uparrow\uparrow}$  this effect is not visible because it is dominated by the coherent contribution. This is expected from the Bloch spectral function in Fig. 2, which shows a very small broadening of the majority  $\Delta_1$  band at the Fermi-energy, indicating a weak scattering and thus a mainly coherent transport. On the other hand, the minority bands show a strong broadening and are therefore strongly affected by scattering leading to a mostly diffusive transport (compare Fig. 4). The redistribution increases the overlap between the states contributing in  $T_{\uparrow\uparrow}$  and  $T_{\downarrow\downarrow}$  which causes the observed increase in  $G_{ap}$  compared to the pure materials.

Consequently, the striking concentration dependence at zero bias is a result of including disorder in the description. It cannot be reproduced by approximating the alloy with an “ordered alloy”<sup>22</sup>, i.e. a stacking of atomic Fe and Co layers, which has not been observed in experiments. Obviously, omitting the diffusive contributions (i.e. neglecting the NVC) does not lead to a meaningful result. We remark that the very high TMR values for the pure components depend sensitively on the computational details. In particular, they show a strong variation for the different thicknesses entering in the thickness averaging, e.g. between 1380% and 14300% for Co. This variation decreases with the bias voltage. This sensitivity explains some deviations between different values presented in literature. On the other hand, we know from Fig. 3 that small amounts of disorder in the layers or at the interfaces reduce the TMR severely. This makes it very hard to achieve the theoretical values in experiments.

At the large voltage of 0.544 V the current in the P configuration decreases slightly while the current in the AP configuration increases linearly with the Co concentration, leading to a decrease of the TMR. The corre-

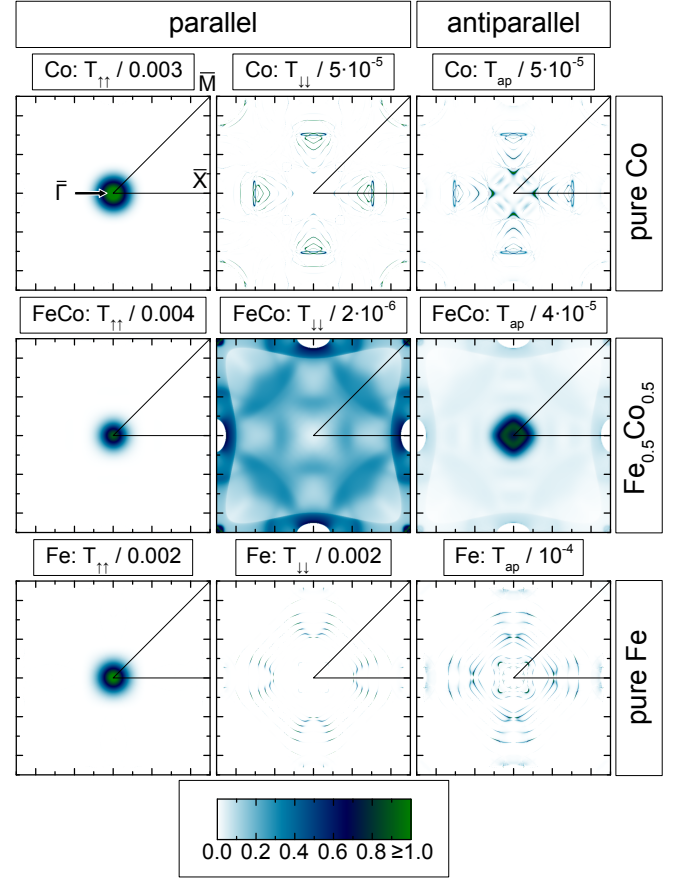


Figure 5. (Color online)  $\vec{k}_{\parallel}$ -resolved transmission  $T_{\sigma\sigma'}(\vec{k}_{\parallel}; E_F)$  at zero bias for junctions containing 20 monolayers Co,  $\text{Fe}_{0.5}\text{Co}_{0.5}$ , or Fe in each ferromagnetic layer (no thickness averaging) at the respective Fermi-energy for the different spin channels. For the AP alignment we show  $T_{ap} = T_{\uparrow\downarrow} + T_{\downarrow\uparrow}$ . Some sharp peaks are clipped to improve the overall visibility. ( $\bar{\Gamma} = \frac{2\pi}{a}(0,0)$ ,  $\bar{X} = \frac{2\pi}{a}(1/2,0)$ , and  $\bar{M} = \frac{2\pi}{a}(1/2,1/2)$ )

sponding conductances are shown in Fig. 6. The origin of this dependence is very different from that at zero bias. The concentration dependence of the AP current, which primarily determines that of the TMR, is governed by the  $\downarrow\uparrow$  channel. The origin of this dependence is related to the position of the Fermi-energy relative to the  $\Delta_1$ -half-metallic region. This will be explained in more detail later.

Our results clearly favor small Co concentrations in order to obtain a large TMR. The concentration dependence of the TMR was investigated in recent experiments<sup>23,24</sup>. Both experiments find a drop in the TMR for large Co concentrations in agreement with our prediction. On the other hand, they find a maximum TMR for a Co concentration of about 25% and a decrease towards pure Fe. There are no indications for this decrease in our calculations suggesting that it is caused by an effect, which was not considered. Still, the TMR values in these experiments (up to 500% at low temperature) are



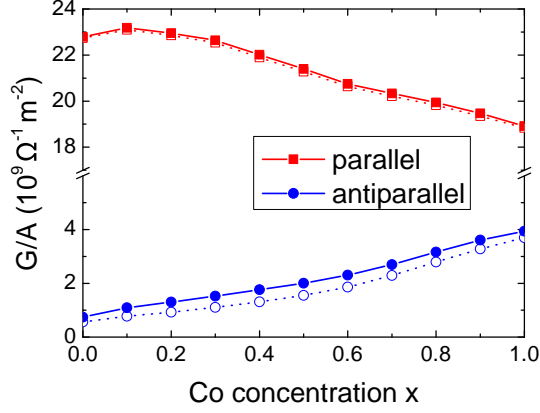


Figure 6. (Color online) Concentration dependence of the conductance in  $\text{Fe}_{1-x}\text{Co}_x/\text{MgO}/\text{Fe}_{1-x}\text{Co}_x$  junctions at a bias voltage  $V = 0.544$  V for P and AP alignment. The dashed lines indicate the dominating contribution, which is the  $\uparrow\uparrow$  channel for P and the  $\downarrow\downarrow$  channel for AP alignment.

a factor of 3-4 smaller than the theoretical predictions. This might be related to an imperfect lattice structure, in particular at the interfaces.

Figure 7 shows the voltage dependence of the TMR for the pure materials and for  $\text{Fe}_{0.5}\text{Co}_{0.5}$  ferromagnetic layers. Since we consider only symmetric junctions, the voltage dependence is symmetric. The strong features at low bias for pure Fe and Co can be attributed to contributions from tunneling between quantum well states in the ferromagnetic layers, which were not completely removed by the thickness averaging process. Both pure cases start at very high values, but the TMR value for Co leads decreases much faster with increasing voltage. The TMR value for  $\text{Fe}_{0.5}\text{Co}_{0.5}$  leads is much smaller at zero bias, but it decreases slower with the bias voltage than for Co, and thus eventually becomes larger than the Co value.

To understand these very different behaviors, we analyze the bias voltage dependence of the conductances, which enter in Eq. (1). This is shown in Fig. 8. The conductance for P alignment is roughly constant for all three considered junctions. The conductance for AP alignment, on the other hand, shows a very different voltage dependence for the three materials. For Co leads the AP conductance increases exponentially beyond a certain threshold voltage and approaches the P value for large voltages. This explains why the TMR drops so drastically for this junction. As explained above, the AP conductance at zero bias in junctions with  $\text{Fe}_{0.5}\text{Co}_{0.5}$  leads is twice as large as for the pure materials. Nevertheless, the increase with the bias voltage is much slower than for pure Co. Therefore, the Co AP conductance exceeds the  $\text{Fe}_{0.5}\text{Co}_{0.5}$  value at 0.3 V leading to the observed reversal in the TMRs. In comparison, the increase in the AP conductance for Fe leads by a factor of 2.6 is rather

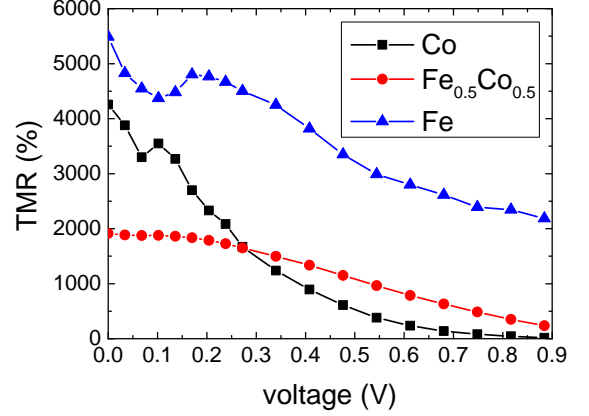


Figure 7. (Color online) Bias voltage dependence of the TMR in junctions with Fe,  $\text{Fe}_{0.5}\text{Co}_{0.5}$ , and Co.

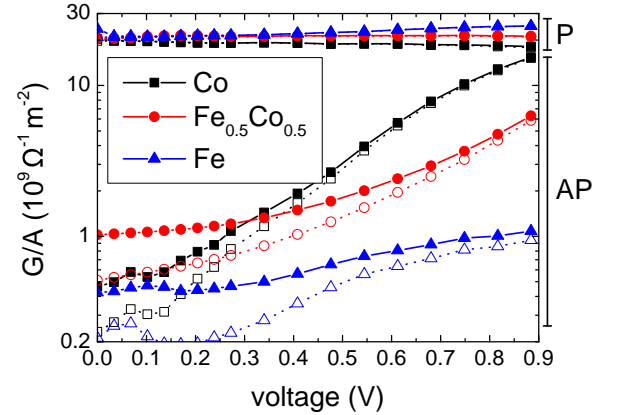


Figure 8. (Color online) Bias voltage dependence of the conductances in junctions with Fe,  $\text{Fe}_{0.5}\text{Co}_{0.5}$ , and Co. The upper lines are for P and the lower lines for AP magnetizations. The dashed lines indicate the dominating contribution, which is the  $\uparrow\uparrow$  channel for P and the  $\downarrow\downarrow$  channel for AP alignment.

small, inducing a moderate decrease in the TMR.

We now explain the reason for the strong increase of the AP current for Co leads. For convenience we consider the case of a negative bias voltage, i.e. the electrons are moving left to right. The increase in  $I_{ap}$  in this case is caused by an increase in the  $I_{\uparrow\downarrow}$  channel. As illustrated in Fig. 9, the applied voltage changes the band alignment in the two ferromagnetic leads. Furthermore, states from a larger energy range contribute to the current (Eq. (2)). At zero bias we have  $\mu_L = \mu_R = E_F$  thus only states from the  $\Delta_1$ -half-metallic region contribute. In particular, majority  $\Delta_1$  states cannot contribute for AP alignment, since they are reflected by the other lead. Increasing the negative bias voltage gradually closes the gap between the majority  $\Delta_1$  states in the left lead and the minority  $\Delta_1$  states in the right lead. For Co the gap

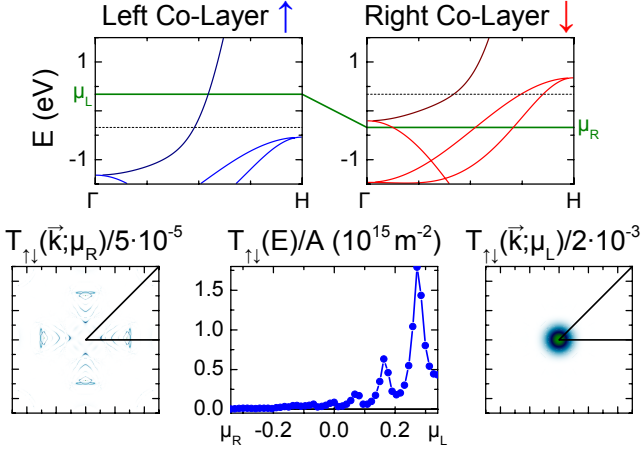


Figure 9. (Color online) Top: band alignment for a junction containing 20 monolayers Co (no thickness averaging) with AP magnetizations in the  $\uparrow\downarrow$  channel at a bias voltage of  $V = (\mu_R - \mu_L)/e = -0.680$  V. The conduction electrons are moving left to right. Bottom: energy resolved conductance (middle) and  $\vec{k}_{\parallel}$ -resolved conductance at  $E = \mu_L$  and  $E = \mu_R$  (left and right) in this channel.

is closed at a voltage of  $-(E_{\Delta_1\downarrow} - E_F)/e = -0.134$  V, where  $E_{\Delta_1\downarrow}$  is the energy of the minority  $\Delta_1$  band at the  $\Gamma$  point. For larger negative voltages an increasing number of  $\Delta_1$  states contributes to the current in the  $\uparrow\downarrow$ -channel, leading to the observed increase of the AP current for Co leads. As an example, Fig. 9 shows the band alignment and the contributing energy range for a large negative voltage. The energy resolved transmission clearly shows the onset of the  $\Delta_1$  contribution. This is superimposed by strong oscillations from quantum well states. Additionally, we show the  $\vec{k}_{\parallel}$  resolved transmission at both endpoints of the energy range. The transmission at  $\mu_L$  shows the dominant peak at  $\bar{\Gamma}$  from the  $\Delta_1$  states, this is not present at  $\mu_R$ , which is below the right minority  $\Delta_1$  band. For large positive voltages the same effect occurs in the  $I_{\downarrow\uparrow}$  channel.

For Fe the Fermi-energy is in the middle of the  $\Delta_1$ -half-metallic region and we have  $(E_{\Delta_1\downarrow} - E_F)/e = 1.36$  V. Thus, the gap is not closed and we do not get large contributions from a  $\Delta_1$ -metallic region to the AP current within the considered voltage range. The  $\text{Fe}_{0.5}\text{Co}_{0.5}$  alloy is an intermediate case. Because of the broadening it is difficult to define the bottom of the  $\Delta_1$  band (Fig. 2). From the conductance (Fig. 8) we find that the onset of the  $\Delta_1$  contributions is delayed compared to Co and much smoother.

The voltage dependence of the TMR for Fe and (bcc) Co leads was investigated experimentally<sup>37</sup>. They find that the TMR decreases faster with the bias for Co than for Fe, in agreement with our results. However, for Fe the experiment shows a stronger decrease than our calculation. This indicates additional inelastic effects in particular for higher voltages. Therefore, in future investigations we plan to include the description of inelastic effects.

The explanation presented in this section is partially in agreement with the one found in Ref. 24. In addition to the contributions from the  $\Delta_1$ -metallic region, they propose a strong influence of an interface resonance state (IRS), which crosses the Fermi-energy from above with increasing Co concentration. In our calculations we do not see convincing evidence for this effect. We observe the IRS, which is at the Fermi-energy in pure Fe. This IRS leads to an enhancement in the  $\downarrow\downarrow$  channel<sup>6</sup>. This is visible in Fig. 5 and 8. However, we find that this contribution drops quickly with increasing voltage and Co concentration. Additionally, this IRS also leads to an increase in the AP conductance and both partially cancel in the TMR. Thus, our calculations indicate that, for the considered barrier thickness of 6 monolayers with perfect interfaces, the IRSs are of minor importance. However, a dedicated *ab initio* study might be advisable to clarify the effect of the IRS.

To summarize, we find that different effects control the TMR at zero and large bias. At zero bias the chemical disorder leads to an increase in the AP conductance and thus a decrease in the TMR for finite concentrations. Even small amounts of disorder suffice to reduce the TMR to values around 2000%. At large bias the TMR is controlled by the onset of contributions from a  $\Delta_1$ -metallic region to the AP current. The threshold voltage for these contributions is determined by the distance between the minority  $\Delta_1$  band and the Fermi-energy, which decreases with the Co concentration. Therefore, the TMR decreases with the Co concentration. The main effect of the disorder in this case is to smoothen the onset. In real junctions one can expect that additional disorder smooths out the peaks in the TMR for small concentrations and small voltages. In this case, the concentration dependence at small bias would qualitatively follow the one found at the higher voltage.

## B. Spin-Transfer Torque

The underlying mechanisms that determine the spin-transfer torque (STT) in FeCo/MgO/FeCo tunnel junctions are closely related to those responsible for the high TMR. The spin-polarized current through the barrier is dominated by  $\Delta_1$  electrons. This leads to a STT which is restricted to the interface<sup>17</sup> (see also Fig. 12). The reason is that the precession of the transport electron is a superposition of the propagating majority and the evanescent minority state. This leads to a decaying precession so that the torque is restricted to the interface. In all-metallic systems the restriction to the interface occurs due to dephasing<sup>38,39</sup>. Dephasing arises from the different precession frequencies of the contributions from the entire Brillouin zone. However, in tunnel junctions there is only a small number of contributing states and dephasing is weak. Therefore, the half-metallic nature of FeCo with respect to the dominating  $\Delta_1$  states is important for the STT in such junctions.

Figure 10 shows our *ab initio* results for the STT obtained from Eq. (3) as a function of the applied bias voltage for junctions I to III. Note that the voltage is going up to  $\pm 0.9$  V and therefore further than in our previous study<sup>17</sup> for pure Fe. As in previous studies, we find a simple bias dependence for pure iron layers. The in-plane torque is almost perfectly linear while the out-of-plane torque is quadratic. Actually, a convincing fit in the presented voltage range requires a biquadratic polynomial  $\tau_{op}(V) \approx a + bV^2 + cV^4$ . For pure cobalt we get a similar behavior for small voltages but strong deviations from the simple dependence at larger voltages. In particular, for the in-plane STT we find a strong reduction for large positive bias and an enhancement for large negative bias. These deviations are the result of contributions from the  $\Delta_1$ -metallic regime to the AP current (compare Sec. III A). The latter lead to a large and highly spin-polarized AP current, which cancels (adds up) with the spin-polarized P current for positive (negative) bias.

Figure 10 includes the bias dependence for junction III with disordered Fe<sub>0.5</sub>Co<sub>0.5</sub> layers. We find almost the simple behavior of pure iron with only small deviations at larger voltages, which are weaker and smoother compared to pure cobalt. In this computationally very demanding calculation, we omit the thickness averaging. The disorder in Fe<sub>0.5</sub>Co<sub>0.5</sub> reduces the quantum well effects, only small residual oscillations are visible. The smooth bias dependence can be explained directly by looking at the Bloch spectral density of Fe<sub>0.5</sub>Co<sub>0.5</sub>, which is shown in Fig. 2. It shows a strong broadening for some of the bands caused by the disorder scattering. In particular the minority  $\Delta_1$  band shows a strong broadening. This leads to a smooth transition from the  $\Delta_1$ -half-metallic to the  $\Delta_1$ -metallic regime and thus explains the smooth onset of the deviations (as explained in Sec. III A). Approximating the alloys with “ordered alloys” leads to larger and more complicated deviations (not shown). Therefore, an accurate description of the alloy scattering is necessary

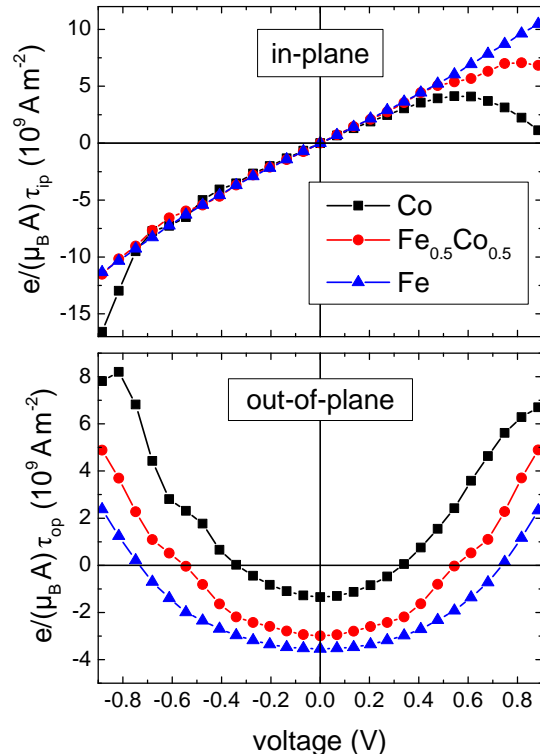


Figure 10. (Color online) In-plane and out-of-plane component of the spin-transfer torque as a function of the applied voltage at a relative angle of  $\theta = 90^\circ$  between the magnetizations for junctions I-III (see Fig. 1), where junction III contains disordered Fe<sub>0.5</sub>Co<sub>0.5</sub> layers.

to obtain the correct voltage dependence.

We find that the STT is of the same order of magnitude for all junctions under investigation. The observed voltage dependence can be qualitatively explained from the band structure or the Bloch spectral density. The bias dependence of the STT using Fe<sub>0.5</sub>Co<sub>0.5</sub> layers is quite similar to that for pure iron layers. Thus, our results can explain the agreement between our previous *ab initio* results<sup>17</sup> and the experiment<sup>13</sup> although both investigations use different ferromagnetic materials.

To provide a quantitative explanation, the in-plane component of the STT can be described by a simple expression in terms of spin currents<sup>15,40</sup>. If the current in the left (right) ferromagnetic lead is determined far enough from the barrier, its polarization will be aligned with the local magnetization and we can define the spin current as  $I_{L(R)}^s = I_{L(R)}^\uparrow - I_{L(R)}^\downarrow$ . By conservation of angular momentum, the difference in the spin currents in right and left lead has to be absorbed by the magnetizations and thus creates the STT. This leads to the expression<sup>40</sup>

$$\tau_{ip}(\theta) = \frac{\mu_B}{e} \frac{1}{\sin(\theta)} (I_L^s(\theta) - I_R^s(\theta) \cos(\theta)). \quad (4)$$



The spin currents depend on the relative angle  $\theta$  between the magnetizations. Making use of the general transformation of a spin state under a rotation, this expression can be simplified to a form that only uses the spin currents in the P and AP alignment<sup>40</sup>

$$\tau_{ip}(\theta) = \frac{1}{2} \frac{\mu_B}{e} (I_P^s + I_{AP}^s) \sin(\theta), \quad (5)$$

where the spin currents can be determined from the four spin channels introduced in Sec. II:  $I_P^s = I^{\uparrow\uparrow} - I^{\downarrow\downarrow}$  and  $I_{AP}^s = I^{\uparrow\downarrow} - I^{\downarrow\uparrow}$ . The in-plane component of the STT calculated from the spin currents is compared to the results from Eq. (3) in Fig. 11. We find perfect agreement, except for Co at large negative bias. For this case the contributions to the STT do not completely decay inside the ferromagnetic layer. This can be observed in Fig. 12, which shows the layer-resolved torque for different cases. Thus, the prerequisites of Eq. (4) are not strictly fulfilled. The description in terms of spin currents provides a quantitative explanation of the effects that determine the in-plane STT. The spin currents entering in Eq. (5) are calculated from the data obtained for the TMR in Sec. III A and are shown in Fig. 13. While the spin currents for the P alignment are roughly linear for AP they show a nonlinear increase in negative value, which is strongly enhanced from Fe to  $\text{Fe}_{0.5}\text{Co}_{0.5}$  to Co. This is caused by the increase in the  $\downarrow\uparrow$  ( $\uparrow\downarrow$ ) channel for positive (negative) bias which, as explained in Sec. III A, is due to contributions from a  $\Delta_1$ -metallic regime. This explains the attenuation of the in-plane STT for positive voltages and the enhancement for negative voltage, which is most pronounced for Co. From the derivation and the persuasive agreement in Fig. 11 we can assume that the validity of Eq. (5) will hold for all angles and thus an investigation of the angular dependence is omitted.

The same arguments that lead to Eq. (4) also yield an identity for the out-of-plane component<sup>40</sup>

$$\tau_{op,R} = -\tau_{op,L}, \quad (6)$$

which relates the torques exerted on both ferromagnetic layers. Note that this does not require a symmetric junction. This equation is fulfilled accurately for junctions containing Fe and  $\text{Fe}_{0.5}\text{Co}_{0.5}$  leads, but only for low voltages in junctions with Co leads, because for higher voltages the contributions to the torque do not fully decay inside the ferromagnetic lead (Fig. 12).

To gain insight into the concentration dependence of the STT we calculate an expansion about zero bias for the full range. This is obtained from a quadratic fit in a small voltage range ( $\pm 68.0$  mV) and shown in Fig. 14. As expected, the in-plane component is zero for all concentrations. We find that the out-of-plane component (i.e. the interlayer exchange coupling) decreases in negative value with the Co concentration. The first derivative of the out-of-plane component is zero by symmetry and for the in-plane component it is constant. This has already been noted above and has important implications for optimizing devices. The second derivative determines the

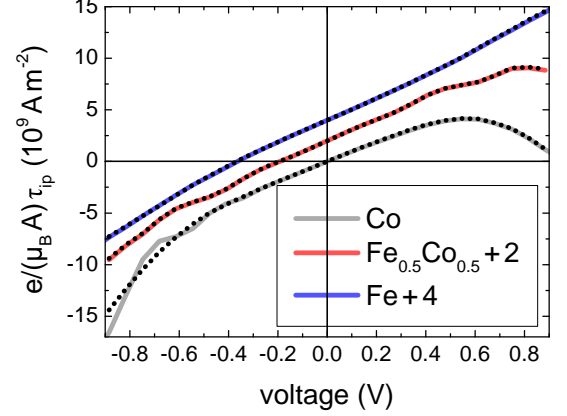


Figure 11. (Color online) Comparison of the in-plane component of the spin-transfer torque calculated from the non-equilibrium density using Eq. (3) as in Fig. 10 (solid) and from the spin currents using Eq. (5) (dotted). The curves are shifted to improve visibility.

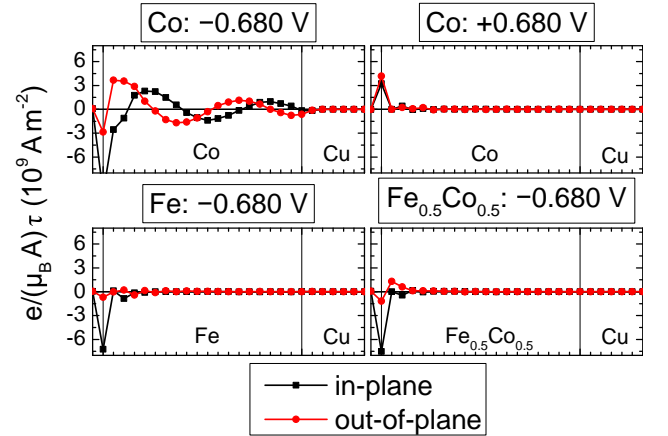


Figure 12. (Color online) Layer resolved in-plane and out-of-plane component of the spin-transfer torque in the free layer for different lead materials and bias voltages

quadratic component and thus it is almost zero for the in-plane component. For the out-of-plane component it has the same order for all concentrations and shows a slight increase with the Co concentration.

When we compare these results with the concentration dependence of the TMR at zero bias (Fig. 3), the absence of any large changes between the pure limits and finite concentrations is conspicuous. As shown before, the concentration dependence of the TMR is mostly determined by the AP-conductance, which in turn shows a strong increase from zero to finite concentrations (Fig. 4). However, the STT for small voltages is completely dominated by the  $\Delta_1$  states which determine the P-conductance and are only weakly affected by the alloy concentration. This can also be seen from Eq. (5): The P spin current  $I_P^s$  is

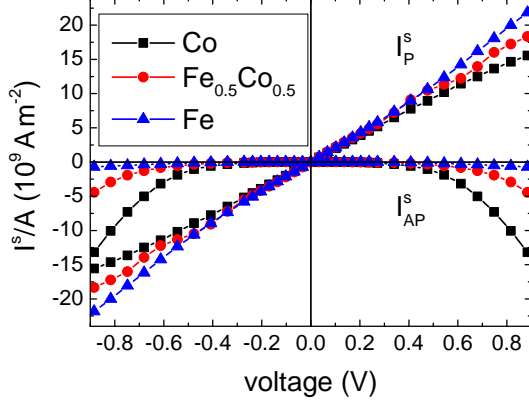


Figure 13. (Color online) Spin currents through the junctions for P and AP alignment.

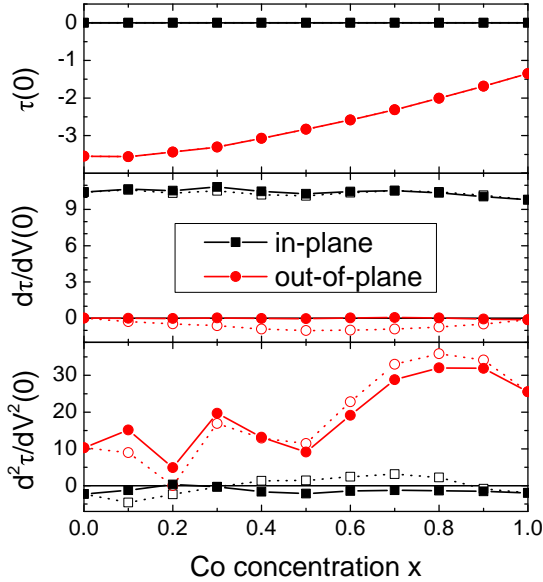


Figure 14. (Color online) Concentration dependent coefficients in an expansion of the spin-transfer torque about zero bias:  $\tau(V) \approx \tau(0) + \frac{d\tau}{dV}(0)V + \frac{1}{2}\frac{d^2\tau}{dV^2}(0)V^2$ . The shown data is scaled with a prefactor  $e/(\mu_B A)$  and has units of  $10^9 \text{ A m}^{-2}$ ,  $10^9 \Omega^{-1} \text{ m}^{-2}$ , and  $10^9 \Omega^{-1} \text{ V}^{-1} \text{ m}^{-2}$ . The dashed lines indicate the results neglecting diffusive contributions.

dominated by the  $\Delta_1$  states, while  $I_{AP}^s$  vanishes at zero bias.

Figure 14 also shows the results obtained without diffusive contributions, i.e. neglecting the NVC. The deviations seem rather small, but from the nonvanishing first derivative of the out-of-plane component we infer that this approximation leads to a systematic error and even to a violation of the symmetry  $\tau_{op}(-V) = \tau_{op}(+V) \Rightarrow$

$\frac{d\tau_{op}}{dV}(0) = 0$ , which follows from Eq. (6) for symmetric junctions.

#### IV. CONCLUSION

Our calculations for the TMR at zero bias show very large values for pure Fe and pure Co leads, which were previously reported in literature. However, even small amounts of chemical disorder caused by alloying lead to a large drop resulting in a TMR of about 2000% for all finite concentrations. This drop is a consequence of the disorder scattering, which leads to a redistribution of the states in  $\vec{k}_{\parallel}$ -space and to an increased overlap of the states in the antiparallel alignment. Since small amounts of disorder are hard to avoid in real junctions, this calculated value might pose a more realistic limit for what can be achieved. Nevertheless, it is still a factor of two larger than current experimental record values.

At a large bias voltage, we find a decrease of the TMR with the Co concentration. This is caused by minority  $\Delta_1$  states, which enter the energy window for transport at high Co concentration and finite bias voltage. This contribution is an inevitable consequence of the band filling and thus the optimum TMR should be found at small to zero Co concentration. This is in contradiction to experimental results<sup>23,24</sup>, which find a maximum TMR for about 25% Co. In our calculations we assume ideal interfaces. Therefore, a possible explanation of this discrepancy is that the quality of the real interfaces depends on the concentration. In this case, a detailed investigation of the concentration dependence of the quality of the interfaces should clarify the discrepancy.

The in-plane (out-of-plane) component of the STT shows the expected linear (quadratic) bias dependence at small voltages. At large voltages and large Co concentrations we find a strong deviation from this simple dependence. By using an expression in terms of the spin-currents in the P and AP alignment, this is traced back to the same effects, which govern the TMR at large voltages. Since the STT at small bias turns out to be mostly independent of the composition the optimization can be focused on the TMR as long as switching can be achieved below the onset of the nonlinear deviations in the voltage dependence.

We find that in all calculations the diffusive contributions (vertex corrections) are important. While for the TMR neglecting them leads to meaningless results, for the STT it leads to relatively small errors, which however break physical symmetries.

#### V. ACKNOWLEDGEMENT

We acknowledge support from DFG grant HE 5922/1-1.

- 
- \* christian.heiliger@physik.uni-giessen.de
- <sup>1</sup> J. S. Moodera, L. R. Kinder, T. M. Wong, and R. Meservey, *Physical Review Letters* **74**, 3273 (1995).
  - <sup>2</sup> T. Miyazaki and N. Tezuka, *Journal of Magnetism and Magnetic Materials* **139**, L231 (1995).
  - <sup>3</sup> S. Yuasa, T. Nagahama, A. Fukushima, Y. Suzuki, and K. Ando, *Nature materials* **3**, 868 (2004).
  - <sup>4</sup> S. S. P. Parkin, C. Kaiser, A. Panchula, P. M. Rice, B. Hughes, M. Samant, and S.-H. Yang, *Nature materials* **3**, 862 (2004).
  - <sup>5</sup> C. Heiliger, P. Zahn, and I. Mertig, *Materials Today* **9**, 46 (2006).
  - <sup>6</sup> W. H. Butler, X.-G. Zhang, T. C. Schulthess, and J. M. MacLaren, *Physical Review B* **63**, 054416 (2001).
  - <sup>7</sup> J. Mathon and A. Umerski, *Physical Review B* **63**, 220403 (2001).
  - <sup>8</sup> J. C. Slonczewski, *Physical Review B* **39**, 6995 (1989).
  - <sup>9</sup> J. C. Slonczewski, *Journal of Magnetism and Magnetic Materials* **159**, L1 (1996).
  - <sup>10</sup> L. Berger, *Physical Review B* **54**, 9353 (1996).
  - <sup>11</sup> D. C. Ralph and M. D. Stiles, *Journal of Magnetism and Magnetic Materials* **320**, 1190 (2008).
  - <sup>12</sup> Z. Diao, Z. Li, S. Wang, Y. Ding, A. Panchula, E. Chen, L.-C. Wang, and Y. Huai, *Journal of Physics: Condensed Matter* **19**, 165209 (2007); J. Z. Sun and D. C. Ralph, *Journal of Magnetism and Magnetic Materials* **320**, 1227 (2008); J. A. Katine and E. E. Fullerton, *Journal of Magnetism and Magnetic Materials* **320**, 1217 (2008).
  - <sup>13</sup> J. C. Sankey, Y.-T. Cui, J. Z. Sun, J. C. Slonczewski, R. A. Buhrman, and D. C. Ralph, *Nature Physics* **4**, 67 (2008).
  - <sup>14</sup> H. Kubota, A. Fukushima, K. Yakushiji, T. Nagahama, S. Yuasa, K. Ando, H. Maehara, Y. Nagamine, K. Tsunekawa, D. D. Djayaprawira, *et al.*, *Nature Physics* **4**, 37 (2008).
  - <sup>15</sup> I. Theodonis, N. Kioussis, A. Kalitsov, M. Chshiev, and W. H. Butler, *Physical Review Letters* **97**, 237205 (2006).
  - <sup>16</sup> J. Xiao, G. E. W. Bauer, and A. Brataas, *Physical Review B* **77**, 224419 (2008).
  - <sup>17</sup> C. Heiliger and M. D. Stiles, *Physical Review Letters* **100**, 186805 (2008).
  - <sup>18</sup> C. Wang, Y.-T. Cui, J. Z. Sun, J. A. Katine, R. A. Buhrman, and D. C. Ralph, *Physical Review B* **79**, 224416 (2009).
  - <sup>19</sup> C. Heiliger, P. Zahn, B. Y. Yavorsky, and I. Mertig, *Physical Review B* **72**, 180406 (2005).
  - <sup>20</sup> A. Kalitsov, M. Chshiev, I. Theodonis, N. Kioussis, and W. H. Butler, *Physical Review B* **79**, 174416 (2009).
  - <sup>21</sup> A. H. Khalil, M. D. Stiles, and C. Heiliger, *Magnetics, IEEE Transactions on* **46**, 1745 (2010).
  - <sup>22</sup> X.-G. Zhang and W. H. Butler, *Physical Review B* **70**, 172407 (2004).
  - <sup>23</sup> Y. M. Lee, J. Hayakawa, S. Ikeda, F. Matsukura, and H. Ohno, *Applied physics letters* **90**, 212507 (2007).
  - <sup>24</sup> F. Bonell, T. Hauet, S. Andrieu, F. Bertran, P. Le Fevre, L. Calmels, A. Tejada, F. Montaigne, B. Warot-Fonrose, B. Belhadji, *et al.*, *Physical Review Letters* **108**, 176602 (2012).
  - <sup>25</sup> H. L. Meyerheim, R. Popescu, J. Kirschner, N. Jedrecy, M. Sauvage-Simkin, B. Heinrich, and R. Pinchaux, *Physical Review Letters* **87**, 076102 (2001).
  - <sup>26</sup> J. Zabloudil, R. Hammerling, L. Szunyogh, and P. Weinberger, *Electron Scattering in Solid Matter: A Theoretical and Computational Treatise*, Springer Series in Solid-State Sciences, Vol. 147 (Springer, 2005) p. 379.
  - <sup>27</sup> J. S. Faulkner and G. M. Stocks, *Physical Review B* **21**, 3222 (1980).
  - <sup>28</sup> C. Franz, M. Czerner, and C. Heiliger, “Implementation of non-equilibrium vertex corrections in KKR: transport through disordered layers,” (2013), arXiv:1305.2399 [cond-mat.mes-hall].
  - <sup>29</sup> B. Velický, *Physical Review* **184**, 614 (1969).
  - <sup>30</sup> Y. Ke, K. Xia, and H. Guo, *Physical Review Letters* **100**, 166805 (2008).
  - <sup>31</sup> C. Heiliger, M. Czerner, B. Y. Yavorsky, I. Mertig, and M. D. Stiles, *Journal of Applied Physics* **103**, 07A709 (2008).
  - <sup>32</sup> J. Henk, A. Ernst, K. K. Saha, and P. Bruno, *Journal of Physics: Condensed Matter* **18**, 2601 (2006).
  - <sup>33</sup> P. Bruno, *Physical Review B* **49**, 13231 (1994).
  - <sup>34</sup> P. M. Haney, C. Heiliger, and M. D. Stiles, *Physical Review B* **79**, 054405 (2009).
  - <sup>35</sup> P. M. Haney, D. Waldron, R. A. Duine, A. S. Núñez, H. Guo, and A. H. MacDonald, *Physical Review B* **76**, 024404 (2007).
  - <sup>36</sup> C. Heiliger, P. Zahn, B. Y. Yavorsky, and I. Mertig, *Physical Review B* **77**, 224407 (2008).
  - <sup>37</sup> S. Yuasa, A. Fukushima, H. Kubota, Y. Suzuki, K. Ando, *et al.*, *Applied Physics Letters* **89**, 042505 (2006).
  - <sup>38</sup> M. D. Stiles and A. Zangwill, *Physical Review B* **66**, 014407 (2002).
  - <sup>39</sup> M. Stiles and J. Miltat, in *Spin Dynamics in Confined Magnetic Structures III*, Topics in Applied Physics, Vol. 101, edited by B. Hillebrands and A. Thiaville (Springer Berlin Heidelberg, 2006) pp. 225–308.
  - <sup>40</sup> J. C. Slonczewski, *Physical Review B* **71**, 024411 (2005).